© EARSeL and Warsaw University, Warsaw 2005. *Proceedings of 4th EARSeL Workshop on Imaging Spectroscopy. New quality in environmental studies.* Zagajewski B., Sobczak M., Wrzesień M., (eds)

COMBINING PASSIVE HYPERSPECTRAL IMAGERY AND ACTIVE FLUORESCENCE LASER SPECTROSCOPY FOR AIRBORNE QUANTITATIVE MAPPING OF OIL SLICKS AT SEA

Marc Lennon[1,2], Sergey Babichenko[3], Nicolas Thomas[1], Vincent Mariette[1], and Grégoire Mercier[2]

1. SAS ActiMar, 24 quai de la Douane, 29200 Brest, France; marc.lennon@actimar.fr
2. GET/ENST-Bretagne, CNRS UMR 2872 TAMCIC, Technopôle Brest-Iroise, CS 83818, 29238 Brest Cedex, France; gregoire.mercier@enst-bretagne.fr
3. AS Laser Diagnostic Instruments, 113A Kadaka Str., 12915 Tallin, Estonia; sergeyb@ldi.ee

ABSTRACT

Efficient observation means are required for supporting operational fight against oil pollutions at sea and recovering operations, including reliable choice and guidance of maritime and airborne fighting means. Among the suite of sensors available, the potential of airborne passive hyperspectral imagery and active fluorescence laser systems for remote sensing of oil spills at sea have been studied in the past.

The potential of combining these two kinds of sensors for quantitative mapping of oil slicks at sea and for supporting the recovering operations is proposed for evaluation in that pilot project. Test flights have been carried out over a controlled oil pollution at sea, using an hyperspectral imager (CASI-2) and a Fluorescence Lidar System (FLS-AU) installed onboard a fixed-wing aircraft.

The data processing chain is presented, including local absolute thickness estimation from lidar data, information extraction from hyperspectral CASI images data thanks to the inversion of a simple optical model of light scattering through a thin layer of oil in the water column, as well as data fusion from both sensors allowing high resolution thickness spatial distribution maps to be produced. Location, extents, and volume of the oil spilled are the main useful quantitative parameters estimated from the maps. The ways towards the design of an operational system including both passive and active airborne optical sensors for supporting recovering operations are presented.

INTRODUCTION

In May 2004, three real oil spills at sea have been performed during a three days campaign off the coasts of Britanny, France. The campaign, named DEPOL04, was carried out under the responsibility of the French Navy represented by the CEPPOL (“Commission d'Etudes Pratiques sur les Pollutions”) and of the French Customs, and managed by the CEDRE (“Centre de documentation de recherche et d'expérimentations sur les pollutions accidentelles des eaux”). The potential of airborne passive hyperspectral imagery (i) (ii) and active fluorescence laser systems (iii) (iv) (v) (vi) for remote sensing of oil spills at sea have been studied in the past. This controlled oil pollution offered the opportunity to test and develop an operational system using jointly an hyperspectral imager (CASI-2) and a Fluorescence Lidar System (FLS-AU) (vii) for oil slicks detection and quantitative mapping. That pilot project is conducted by ActiMar[1], a French SME specialized in opera-

[1] http://www.actimar.fr

tional oceanography and high resolution remote sensing, in collaboration with GET/ENST-Bretagne (TIME team, CNRS UMR 2872 TAMCIC), and is funded by the RITMER program of the French Ministry of Research under the name “DETECSUIV”. Radar satellites as well as airborne reconnaissance missions are used to obtain oil slicks localization (viii). Flight lines are prepared and integrated into a flight assistance system. CASI-2 and FLS-AU are installed onboard a fixed-wing aircraft (Cessna 404). Using an optimal flight configuration, 10 to 40 km² per hour can be recorded. The whole operational aspects of the campaign can be found in (ix).

In order to extract the useful parameters from CASI-2 and FLS-AU data, a specific processing chain is developed. CASI data allow high spatial resolution (1 and 2 meters) slicks maps to be produced, and the polluted surface to be estimated, after illumination corrections and definition of specific colour spaces taking advantage of observed spectral phenomena. Two CASI-2 configurations have been tested, including 18 and 32 spectral bands. The data acquisition campaign has been completed with spectroscopic measurements on the slicks at sea, onboard a small infloatable boat. A simple optical model of light scattering in the water column is presented and is shown to be relevant for understanding the intra-slick spectral variability.

In-lab calibration of fluorescence spectra acquired by FLS allows thickness to be locally estimated. Those measurements are used to “calibrate” the CASI data and to extend the estimation of thickness over all the CASI pixels. That data fusion procedure is shown to be consistent with the optical model over a polluted water area including a thin layer of oil, and allows very high spatial resolution (1 meter) thickness distribution maps to be computed. Those maps show the spatial distribution of the oil thickness and allow the volume of oil spilled to be estimated. In order to show all the data processing steps, a demonstrator has been developed, starting from raw CASI-2 and FLS-AU data integration and fusion up to the visualization of high spatial resolution oil thickness maps and oil pollution quantitative results.

The potential and the limits of the whole approach are discussed, regarding the parameters estimation quality. Recommendations are made for the use of those combined sensors as a reliable observation mean for supporting operational recovering operations at sea.

DATA PROCESSING

CASI data processing chain

a. Schematics

The joint use of two sensors implies to consider the limitations of both. For a single CASI data acquisition, the flight altitude should be maximized in order to reach the maximum swath if the meteorological conditions are adequate. In the present case, the flight altitude is limited by the maximum flight altitude of the FLS-AU, which is equal to 500m (about 1500ft). The speed of the acquisition should be minimized in order to acquire the maximum amount of data. The minimum speed is however limited by the capabilities of the platform. Using a Cessna 404, this minimum speed is fixed at 100kt. to avoid turbulences. Considering those flight parameters, the CASI-2 configuration over its 400-1000nm spectral range is the following:

- number of spectral bands: 18 (equally distributed over the spectral range)
- spectral resolution: 30nm
- spatial resolution: 1m
- swath: 380m

The whole processing chain of CASI dataset is shown on Figure 1.

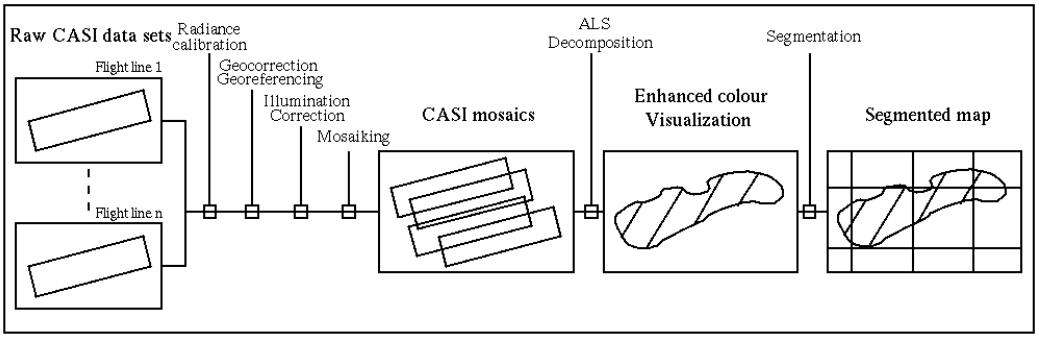

Figure 1: CASI data processing chain

b. Preprocessing

Raw CASI data are calibrated into radiance units, geometrically corrected and georeferenced thanks to INS/dGPS data. Across-track illumination corrections are performed, and a mosaic of flight lines is built. Examples of CASI spectra recorded over clear water, thin and thick oil films, during the DEPOL04 experiment are presented in the next paragraph.

c. "Physical" feature extraction

Standard radiative transfer modelling over sea water leads to the following expression for at-sensor observed radiance $L(\lambda)$ (x):

$$L(\lambda) = L_{atm}(\lambda) + L_g(\lambda)T_u(\lambda) + L_w(\lambda)T_u(\lambda)$$

with $L_{atm}(\lambda)$: path radiance of atmosphere; $L_g(\lambda)$: radiance from contribution of specular reflections on the sea surface; $L_w(\lambda)$: water-leaving radiance; $T_u(\lambda)$: upwelling transmittance of the atmosphere.

The DEPOL04 experiment has shown that (independently from waves sunglint) the global energy reflected by an oil polluted surface is greater than the energy reflected by surrounding clear water because of daily greater specular reflection on the oil surface from the sun (Figure 2 left). From that observation, the global reflected energy (or "lightness" L) can be computed as an extension of the lightness used in the standard RGB to HLS colour transform. For each pixel, L is then evaluated as the integration of the radiance $L(\lambda)$ over the whole spectral range:

$$L = \frac{\int_{\lambda_{min}}^{\lambda_{max}} L(\lambda)d\lambda}{\lambda_{max} - \lambda_{min}}$$

Intra-slick intrinsic spectral variability can now be analyzed by removing lightness from the observation, leading to the 'lightness-free" radiance $S(\lambda)$:

$$S(\lambda) = L(\lambda) - L$$

CASI experiments over the slicks spilled from the *PRESTIGE* tanker in 2002 (ii), as well as the current DEPOL04 experiment, have shown that the spectral behaviour of $S(\lambda)$ depending on oil thickness on the surface is the following : while the oil layer becomes thicker, the radiance decreases in the blue and increases in the near infrared part of the electromagnetic spectrum, leading to the so-called "spectral rotation" around 600 nm as a function of oil thickness (Figure 2 right)

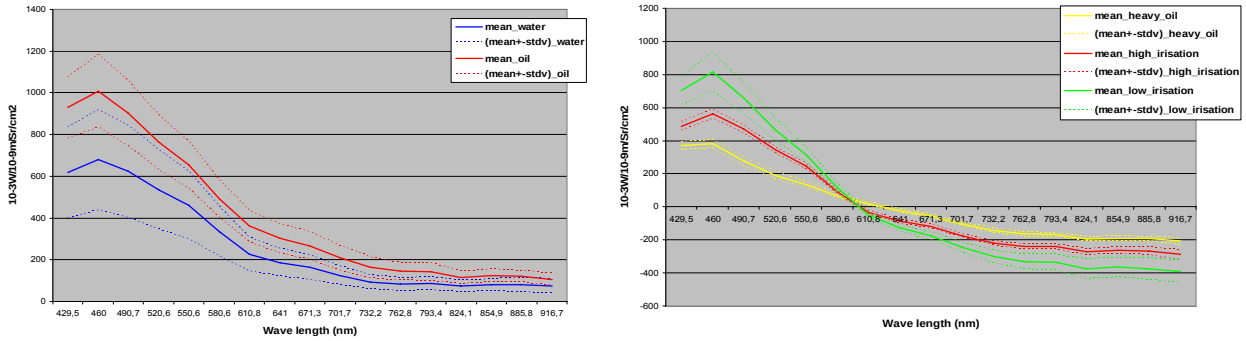

Figure 2: (left) Radiances L(λ) as observed by CASI from clear water and oil polluted surfaces; (right) "Spectral rotation" as observed on "lightness-free" CASI spectra from different oil films

In order to understand the "spectral rotation phenomenon", let consider the optical model of multiple reflections within two plane interfaces (Figure 3) (xi).

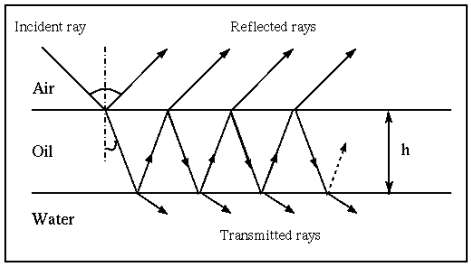

Figure 3: Multiple reflections across an oil film as described by a thin layer optical model

In the case of a thin layer of oil floating on the sea surface, the optical model describes the interferences induced by multiple reflections and transmissions of an incident plane electromagnetic wave coming across the oil layer separating the air and water, all of them fitted with different refraction indices. For the purpose of simulations, let take the simple case of an incident electromagnetic wave orthogonal to the oil slick floating on the sea surface. The reflectance of oil surface can be easily computed and leads to the following expression:

$$R = \left(\frac{n-1}{n+1}\right)^2 \frac{1+\left(\frac{n-n_1}{n+n_1}\frac{n+1}{n-1}\right)^2 - 2\left(\frac{n-n_1}{n+n_1}\frac{n+1}{n-1}\right)\cos(4nk_0h)}{1+\left(\frac{n-n_1}{n+n_1}\frac{n-1}{n+1}\right)^2 - 2\left(\frac{n-n_1}{n+n_1}\frac{n-1}{n+1}\right)\cos(4nk_0h)}$$

with R: reflectance of the oil slick; n and n_1: refraction indices of oil and water; k_0: air wavenumber; h : oil thickness. Using this expression with standard parameters of oil and water refraction indices, the radiance above the oil surface $L_g(\lambda)$ can be computed:

$$L_g(\lambda) = L_{sol}(\lambda)\, R$$

with $L_{sol}(\lambda)$: direct sunlight radiance on the surface. A real spectra of $L_{sol}(\lambda)$ has been measured on the slick onboard a small infloatable boat jointly with CASI data acquisition and is used here for the simulation of $L_g(\lambda)$. From $L_g(\lambda)$, "lightness-free" radiances $S_g(\lambda)$ are simulated, parameterized by a range of thicknesses h. The results of those simulations are shown on Figure 4 (left).

It has to be noticed from Figure 4 (left) that the "spectral rotation" as a function of oil thickness is revealed by the simulation. The differences in the spectral shapes of simulated lightness-free oil slick radiance $S_g(\lambda)$ (Figure 4 left) and computed lightness-free at-sensor radiance $S(\lambda)$ (Figure 2 right) are mainly due to the atmospheric transmittance $T_u(\lambda)$ and path radiance $L_{atm}(\lambda)$ that do not affect the spectral rotation phenomenon. Water-leaving radiance can be considered as not significant for comparison purposes.

Those previous simulations show that the "spectral rotation" observed on CASI data is directly induced by the oil thickness. Following that observation, the spectral rotation can be first simply quantified by the L_2 norm of $S(\lambda)$. It has to be noticed that the L_2 norm can be seen as an extension of the "saturation" used in the standard RGB to HLS colour transform. For each pixel, S is then evaluated by the following expression:

$$S = \|S(\lambda)\| = \sqrt{\int_{\lambda_{min}}^{\lambda_{max}} S^2(\lambda) d\lambda}$$

From a physical point of view, the dynamical range of the saturation S is however still dependent on the lightness L. In order to avoid that dependence, the cosine of the spectral angle between the observed radiance $L(\lambda)$ and the unit vector is computed using the following expression:

$$A = \sqrt{\lambda_{max} - \lambda_{min}} \frac{L}{\|L(\lambda)\|}$$

The simulation of A as a function of the thickness h, using standard parameters of oil and water refraction indices, is shown on Figure 4 (right). It has to be noticed that, for low thicknesses, the parameter A is quasi-linearly related to the thickness h, following the thin oil layer model configuration in the simple case of an incident electromagnetic wave orthogonal to the oil slick floating on the sea surface. In real observations however, refraction indices as well as atmospheric parameters remain unknown, but the quasi-linear relationship remains however valid. Keeping the approximation of orthogonality in mind, this property will enable the parameter A to be related to the absolute thickness measurements estimated from the lidar dataset.

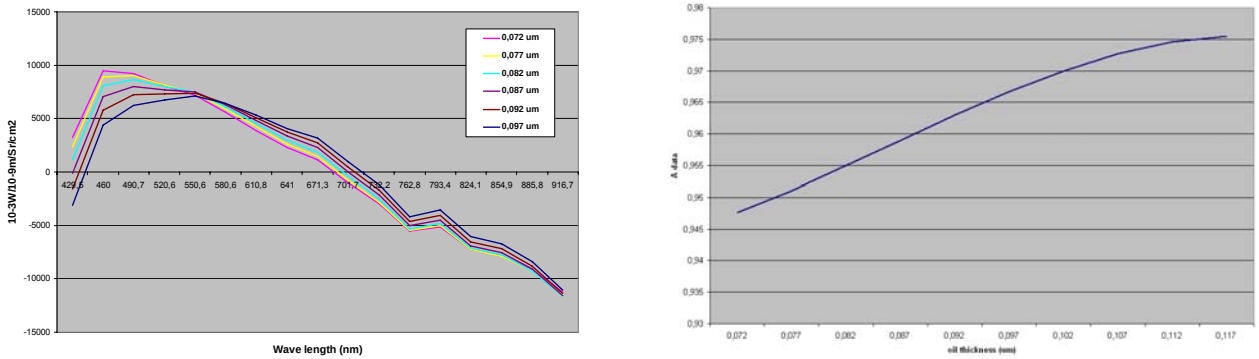

Figure 4: (left) "lightness-free" oil radiance spectra Sg(λ) simulated for different oil thicknesses; (right) Simulation of parameter A as a function of the thickness h

The 3 parameters A (related to thickness), L (related to the surface reflexion), and S (related to intra-slick variability dependent on the lightness) extracted from the CASI data allow the whole CASI dataset to be reduced to 3 dimensions with a physical meaning. That "ALS decomposition" can be used for further enhanced visualization of the data (Figure 9), as well as in the segmentation and data fusion processes.

d. Segmentation

ALS decomposition allows high visual quality images to be produced. In order to avoid false alarms mainly due to sun glint and in order to quickly get an accurate estimation of the polluted surface, the segmentation is currently manually performed on the colour ALS visualization by a visual observer. An example of a segmented oil slick map is shown on Figure 10.

FLS-AU data processing chain

a. Schematics

The FLS-AU fluorescence lidar is an active sensor using Raman and induced fluorescence characteristics of water and oil in order to discriminate both targets, as well as to locally quantify the oil

thickness (vii). FLS-AU is fitted with a 308 nm pulse excimer laser, and a spectral diffraction receiver allowing the signal to be sampled on 500 spectral points over the 300-500 nm spectral range. FLS-AU allows data to be recorded from 50m to 500m flying altitude, with a frequency of 20 Hz. The whole processing chain of FLS-AU dataset is shown on Figure 5.

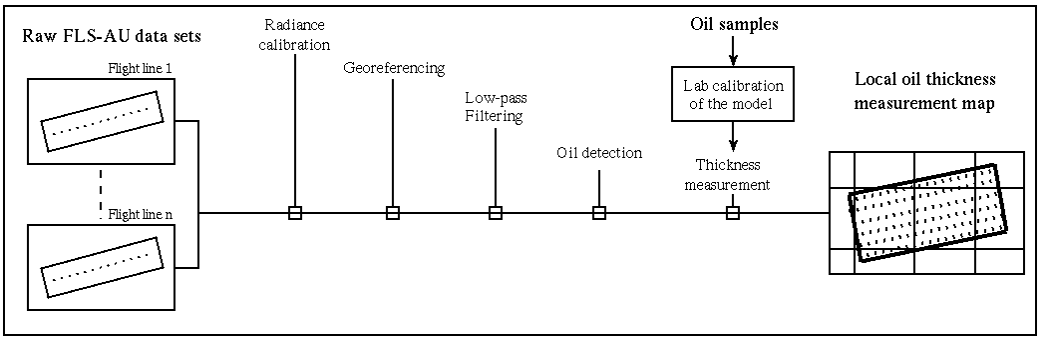

Figure 5: FLS-AU data processing chain

b. Pre-processing

Raw FLS-AU spectra are calibrated into radiance units and georeferenced thanks to handheld GPS data jointly recorded with FLS-AU data. Data are low-pass filtered in order to increase the signal to noise ratio. Along-track sampling is around 25m after the pre-processing steps. Examples of FLS-AU spectra recorded over clear water, thin and thick oil films, during the DEPOL04 experiment are shown on Figure 6 (left). The high differences in Rayleigh scattering (308nm), Raman scattering (around 345nm), as well as in induced fluorescence (over 360nm) are to be noticed.

c. Oil detection

Raman scattering being possibly influenced by external water turbidity factors, only the fluorescence information is used for the detection of oil on the sea surface. A simple threshold on maximal fluorescence is used for decision-making.

d. Local thickness measurements

Fluorescence intensity reaches saturation for quite low oil thicknesses and then becomes independent from the latter. Once oil has been detected on a sample thanks to the fluorescence information, the thickness value is hence computed using only Raman scattering information, thanks to the following empirical model (iii) (iv):

$$d = -\frac{1}{k_e + k_r}\ln\left(\frac{R}{R^*}\right)$$

With d: thickness to be estimated; R^*: Raman scattering; R: Raman scattering over clear water; k_e and k_r: attenuation coefficients at Rayleigh wavelength and Raman wavelength.

Those attenuation coefficients are measured in the laboratory using real oil samples spilled during the DEPOL04 experiment. If not available, those values could be extracted from standard libraries. Spectra used in the lab for calibrating the model are shown on Figure 6 (right). An example of local geographical thickness measurements computed from the FLS-AU data is shown on Figure 11.

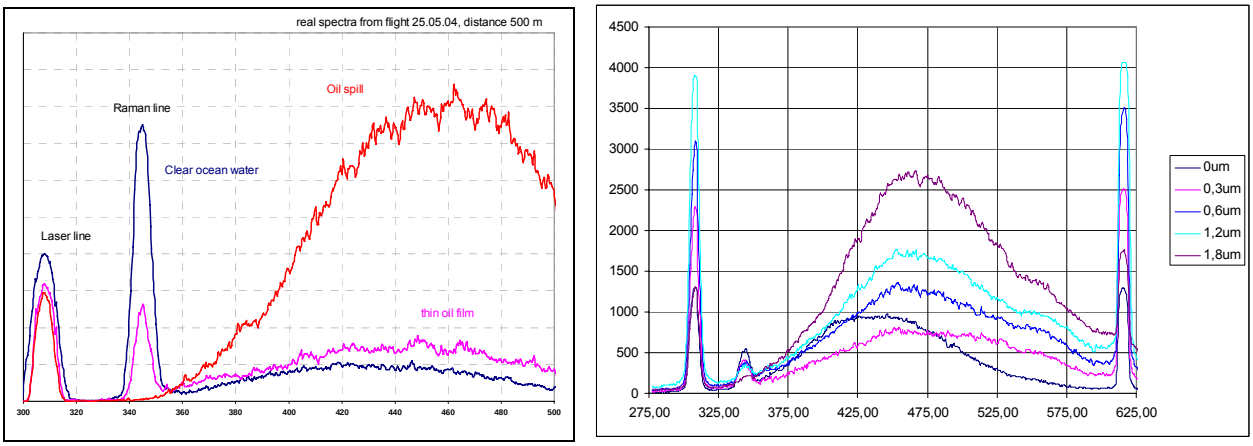

Figure 6: (left) FLS-AU spectra recorded during the DEPOL04 experiment over water and oil films (right) Spectra used in the lab for calibrating the thickness estimation model

Data fusion

a. Schematics

The whole processing chain for CASI + FLS-AU data fusion is shown on Figure 7.

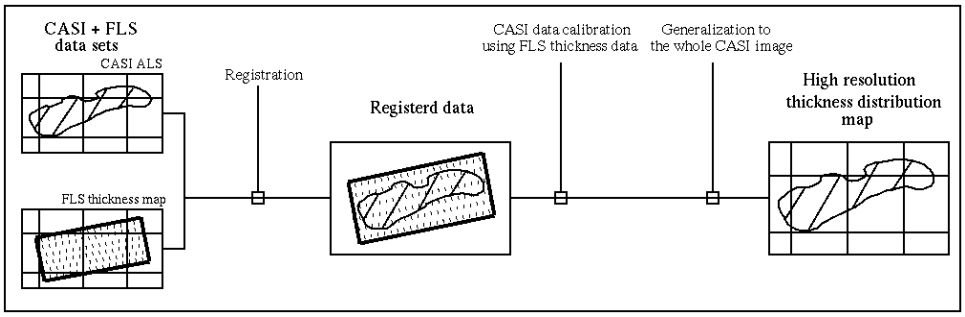

Figure 7: CASI + FLS-AU data fusion chain

b. Data sets registration

Low frequency handheld GPS data jointly recorded with the FLS-AU dataset are temporally interpolated in order to be registered to high frequency/high accuracy data from the INS/dGPS data jointly recorded with the CASI dataset. A high accuracy positioning data is hence associated to each thickness data. Resampling of FLS-AU data over the same grid as CASI data hence leads to the accurate registration of both data sets (Figure 8 left).

c. Data fusion process

It has been shown in a previous paragraph that the parameter *A* extracted from the CASI dataset is quasi-linearly related to the thickness of the oil film on the water surface, over the domain of validity of the thin layer optical model. That relative thickness parameter *A* can hence be calibrated into absolute thickness estimations thanks to the relationship with thickness measurements obtained from the FLS-AU dataset. The two parameters of the linear model are estimated thanks to the correlation of *A* with absolute thickness measurements when available over the same pixels from the FLS-AU dataset (Figure 8 right), and applied over the whole pixels of the CASI data set, in order to get a high resolution thickness spatial distribution map. An example of such a map obtained during the DEPOL04 experiment is shown on Figure 12.

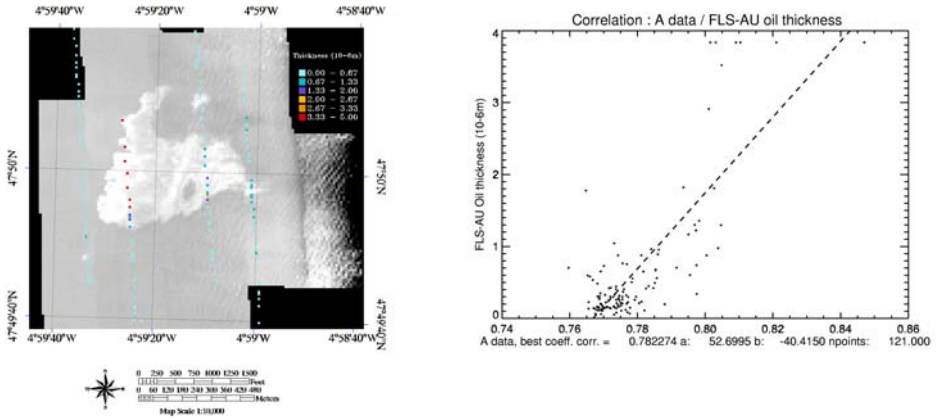

Figure 8: (left) Registration of CASI data with thickness measurements from FLS-AU; (right) Absolute calibration of CASI data using corresponding FLS-AU estimated thicknesses

Quantification of the parameters

Surface and volume are estimated thanks to the integration of local estimated values over the whole pixels of the slick. Examples of quantitative results obtained during the DEPOL04 experiment are given in Table 1.

RESULTS

ALS enhanced visualisation map

An example of a CASI enhanced colour visualization map computed from the ALS decomposition is shown on Figure 9. That map allows one to get a first qualitative assessment of the pollution. The distribution of the volume of the oil is highly revealed in the image (from blue to red). Figure 9 shows that the maximum concentration of oil is located on the west side of the slick in a small area compared to its whole extent. That information is not quantitative but would allow the first fighting means (aerial or maritime) to be guided to the most important part of the polluted area.

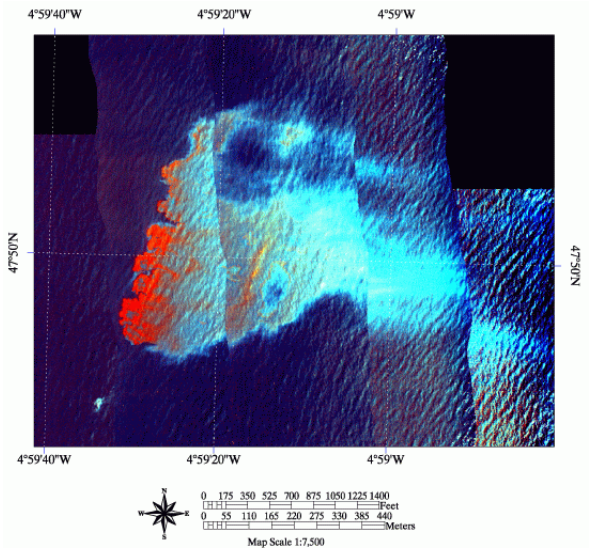

Figure 9: "ALS" enhanced visualization map.

Localization and geographical configuration map

The segmentation of the CASI ALS map is shown on Figure 10. From that map, the accurate localization and geographical configuration of the slick is derived. The exact extents of the slick can be computed.

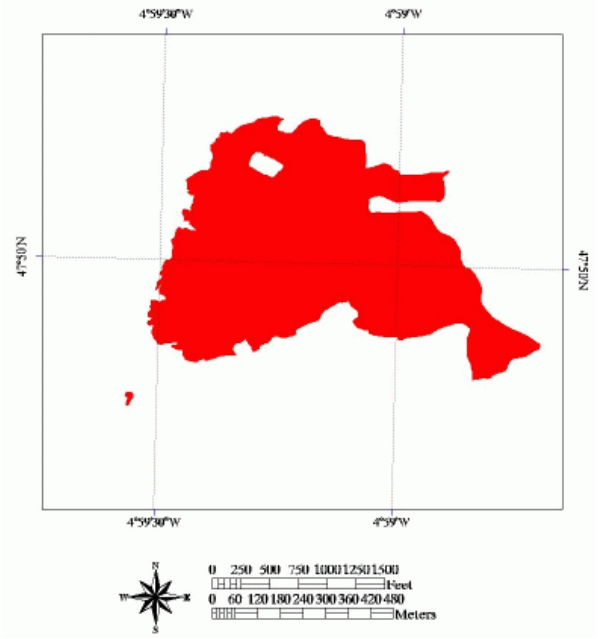

Figure 10: Localization map.

Local oil thickness measurement map

Local geographical thickness measurements computed from the FLS-AU data is shown on Figure 11.

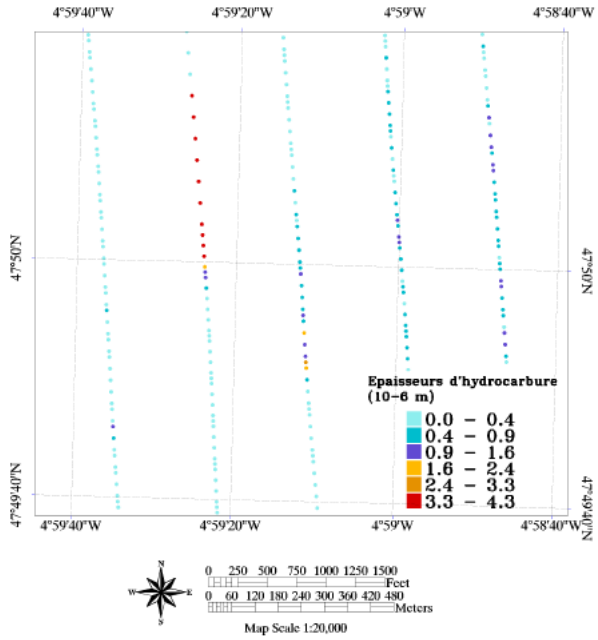

Figure 11: Local oil thickness measurement map.

High resolution thickness distribution map

The CASI-2 and FLS-AU data fusion process leads to the computation of the high resolution thickness distribution map shown on Figure 12. The colours associated to the estimated thicknesses are quantitatively reported in the legend. This map confirms the qualitative assessment of the CASI enhanced visualization map, and allows the whole volume of oil spilled to be estimated.

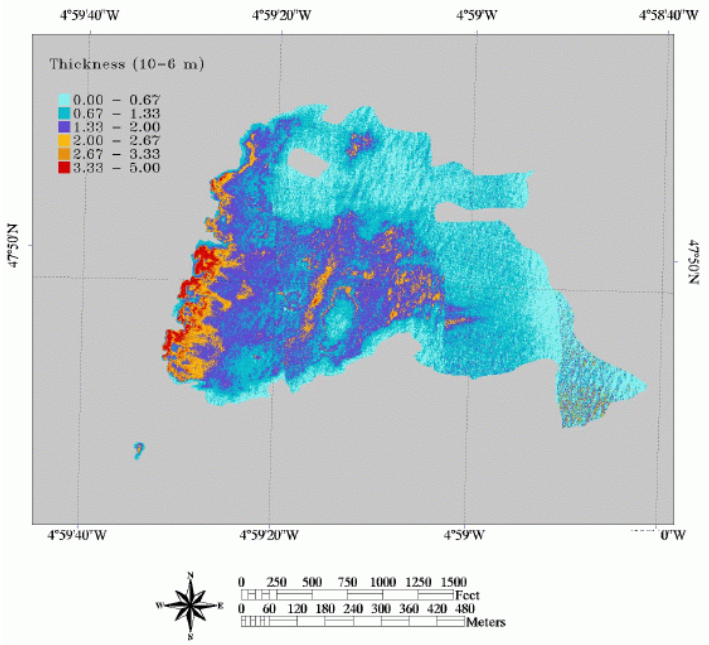

Figure 12: High resolution thickness distribution map.

Quantitative results and critical study

Three 10 m^3 oil slicks, alpha, bravo, and charlie, have been spilled during the DEPOL04 experiment. The alpha slick was crude oil, while bravo and charlie included 65 % HFO + 35 % LCO. The quantitative results are listed in Table 1. The results show that the volumes have been underestimated for each slick, with an error factor ranging approximately from 5 (alpha) to 30 (bravo). Those errors are mainly due to the saturation of the optical measurements (and induced non validity of the optical model used) after a critical thickness which depends on the type of the oil observed. In the current experiment, the FLS-AU measurements were saturated at approximately 10µm for alpha, and 5µm for bravo and charlie. Those saturation threshold differences explain the best estimations over the alpha slick. The estimated thicknesses are quite accurate over thin layers, while saturated over thick layers. The most dispersed the volume is over a large surface, the most accurate the estimation of the volume is. In the current experiment, the slicks were not so much dispersed since data acquisition was performed a few hours after the spill. The system capabilities are hence limited to provide the minimal bound of the real volume of oil spilled, which should however be considered as reliable. It has to be noticed that the high resolution thickness distribution maps allow, despite the saturation areas, the limits of the slick and the spatial distribution of volumes to be reliably represented. Those informations are *a priori* the most important for the support of operational aerial and/or maritime recovering operations.

Table 1: Quantitative results.

Slick	Estimated surface (km²)	Estimated volume (m3)	Volume factor error
Alpha	0.97	2.08	4.8
Bravo	0.34	0.36	27.8
Charlie	0.39	0.49	20.4

CONCLUSIONS

This pilot project allowed us to make a step towards answering environmental concerns associated with accidents in oil storage and transportation. Passive and active hyperspectral sensors have been shown to be complementary. In particular, data fusion from both sensors allows high resolution spatial distribution of oil thickness to be geographically mapped. We think that the use of those

combined sensors as a reliable observation mean for supporting operational recovering operations is a high potential value-added application. A demonstrator including the data processing chain has been developed as a basis for future operational software development.

FURTHER WORKS

Parameterization of the radiative transfer model in the case of an oil slick floating on the ocean still needs improvements. In particular, the thin layer optical model will be used without any approximations, in conjunction with atmospheric parameters and water leaving radiance estimations, in order to simulate the signal reaching the sensor. Sea wave numerical models will be used in order to simulate a whole hyperspectral data cube, and a robust inversion procedure will be constructed. In a near future, the system will be tested on-board an airborne integrated platform, including data communication from the aircraft to the vessels in charge of recovering operations at sea, in order to support the operational fight and the guidance of the vessels.

ACKNOWLEDGEMENTS

The authors would like to thank CEPPOL, Douanes Françaises and CEDRE for having supported and managed the DEPOL04 experiment, and for having accepted our participation. They also would like to thank the RITMER committee from the French Ministry of Research for the financial co-funding of the project, as well as the European Union for co-funding the remote sensing activities at ActiMar through the FEDER (Fonds Européens de Développement Régional) fundings.

References

i Byfield V, 1998. Optical remote sensing of oil in the marine environment. PhD Thesis, Univ. of Southampton, UK.

ii Lennon M, V Mariette, A Coat, V Verbeque, P Mouge, GA Borstad, P Willis, R Kerr & M Alvarez, 2003. Detection and mapping of the November 2002 PRESTIGE Tanker oil spill in Galicia, Spain, with the airborne multispectral CASI sensor. In: 3rd EARSeL Workshop on Imaging Spectroscopy, 13-16 may 2003, Oberpfaffenhofen, Germany, edited by M Habermeyer, A Müller & S Holzwarth (EARSeL, Paris).

iii Reuter R, H Wang, R Willkomm, K Loguay, T Hengstermann & A Braun, 1995. A Laser Fluorosensor for Maritime Surveillance: Measurement of Oil Spills. In: EARSEL Advances in Remote Sensing, 3: 152-169

iv Patsayeva S, V Yuzhakov, V Varlamov, R Barbini, R Fantoni, C Frassanito & A Palucci, 2000. Laser spectroscopy of mineral oils on water surface. In: 4th EARSeL Workshop on Lidar Remote Sensing of Land and Sea, 16-17 June 2000, Dresden, Germany, edited by S Babichenko & R Reuter (EARSeL, Paris).

v Babichenko S, A Dudelzak & L Poryvkina, 2002. Laser sensing technologies in studies of marine and coastal environment. In: The Seventh International Conference on Remote Sensing for Marine and Coastal Environments, Miami, Florida, 20-22 May 2002, eProceedings, Veridan, 8 p.

vi Brown CE & MF Fingas, 2003. Review of the development of laser fluorosensors for oil spill application. Marine Pollution Bulletin, 47: 477-484.

vii Babichenko S, A Dudelzak & L Poryvkina, 2004. Laser remote sensing of coastal and terrestrial pollution by FLS-Lidar. Earsel eProceedings 3, 1/2004.

viii Lennon M, S Babichenko, N Thomas, V Mariette & G Mercier, 2005. Oil slick detection and characterization by satellite and airborne sensors: experimental results with SAR, Hyperspectral and Lidar data. In: IEEE IGARSS' 2005, Seoul, Korea, 25-29 July 2005.

ix Lennon M, N Thomas, V Mariette, S Babichenko & G Mercier, 2005. Operational quantitative mapping of oil pollutions at sea by joint use of an Hyperspectral Imager and a Fluorescence Lidar System on-board a fixed-wing aircraft. In: IEEE OCEANS' 2005, Brest, France, 20-23 June 2005.

x Hochberg EJ, S Andréfouët & MR Tyler, 2003. Sea surface correction of high spatial resolution Ikonos images to improve bottom mapping in near-shore environments. IEEE Tr. Geosciences and Remote Sensing, 41(7): 1724-172.

xi De Beaucoudrey N, P Schott & C Bourlier, 2003. Detection of oil slicks on sea surface depending on layer thickness and sensor frequency. In: IEEE IGARSS' 2003, Toulouse, France, 21-25 July 2003.